A Multi-Level Feature Distribution Learning Method for Automatic Modulation Open-Set Recognition

Zhenxi Zhang, *Member, IEEE*, Haoyue Tan, *Student Member, IEEE*, Xiaoran Shi, *Member, IEEE*, Heng Zhou, *Member, IEEE*, Yun Lin, *Senior Member, IEEE*, Yu Li, *Graduate Student Member, IEEE*, Jiankun Ma, Xueru Bai, *Senior Member, IEEE*, and Feng Zhou, *Member, IEEE*

***Abstract*—The study of open-set recognition for modulation types in communication signals is of high research significance, as it addresses critical challenges in wireless communication systems, such as spectrum monitoring, interference identification, and secure transmission. Traditional closed-set recognition methods are limited to pre-defined modulation types, which restrict their adaptability in real-world environments where new or unknown modulation types may emerge. In contrast, Automatic Modulation Open-Set Recognition (AMOSR) not only classifies known modulation types but also explicitly recognizes unknown ones, thereby addressing the inherent limitations of closed-set approaches. However, existing AMOSR methods face challenges in achieving a balanced optimization between the empirical risk for known modulation types and the open space risk for unknown modulation types. This issue results in two adverse effects: (1) low rejection accuracy for unknown modulation signals, and (2) degraded classification performance on known types due to overfitting to the closed-set training data. To address these issues, we propose a multi-level feature distribution learning (MLFDL) method for AMOSR, which integrates a pseudo modulation placeholder method with feature distribution constraints. To simulate unknown modulation types during training, we introduce a pseudo modulation placeholder via manifold mixup, which constructs synthetic samples in the feature space to approximate the behavior of unseen modulations. We design a multi-level feature distribution constraint method, combining sample-centroid contrastive learning with a max-min feature constraint, ensuring adequate feature space for unknown modulation signals and enhancing the separation between known and unknown signals. Comprehensive experiments across different datasets show that MLFDL achieves state-of-the-art performance on both AUROC and OSCR metrics, with minimum sample-to-centroid distance serving as a robust decision criterion for unknown signal recognition.**

***Index Terms*—Automatic modulation classification, open-set recognition, feature distribution constraint.**

I. Introduction

AUTOMATIC Modulation Recognition (AMR) is widely used in civilian and public security applications, such as cognitive radio, signal reconnaissance, electronic countermeasures, and spectrum sensing [1]. By rapidly identifying transmission signals, AMR enables the timely detection of abnormal signals, helping prevent unauthorized device intrusions, mitigating malicious attacks and data breaches, and ensuring the secure and reliable operation of IoT systems [2]. Deep learning techniques, leveraging their powerful feature extraction capabilities, have significantly enhanced the accuracy of automatic modulation recognition. Approaches based on CNNs [3], [4], LSTMs [5], and Transformers [6] effectively exploit both spatial and temporal correlations in signal data.

Most existing AMR methods operate under a closed-set assumption [7], [8], where all modulation types encountered during testing are assumed to be known and included in the training phase. However, real-world communication environments are complex and often contain unknown or anomalous signals [9], including modulation schemes not seen during training. Conventional closed-set models fail to reject such unknown signals, limiting their practical applicability.

The AMOSR method [10], [11] addresses this challenge by pursuing two critical objectives: effective rejection of unknown modulation types and maintaining high recognition accuracy for known modulation types. By simultaneously achieving these goals, AMOSR enhances overall system reliability while enabling the detection of unknown modulated signals, significantly improving its real-world applicability. These advantages prove particularly important in dynamic communication environments. The main challenge in AMOSR is the absence of

Received 18 April 2025; revised 27 September 2025 and 19 November 2025; accepted 18 January 2026. Date of publication 22 January 2026; date of current version 30 January 2026. This research was supported in part by the National Natural Science Foundation of China under grant number U2541202, 62401429, 62401445, 62501437, 62531020, and 62425113, in part by the Postdoctoral Fellowship Program of CPSF under grant number GZC20241332, GZC20232048, and GZC20251207, in part by the China Postdoctoral Science Foundation under grant number 2024M761178 and 2025M771739, in part by the Fundamental Research Funds for the Central Universities under grant number ZYTS25144, in part by the Seed Funding Project of Sichuan Aerospace Electronics Research Institute under grant number of ZZJJ202402-01, in part by the Funded by Basic Research Program of Jiangsu under grant number BK20251623, and in part by the Jiangsu Funding Program for Excellent Postdoctoral Talent under grant number 2025ZB126. The associate editor coordinating the review of this article and approving it for publication was R. Long. *(Corresponding author: Xiaoran Shi.)*

Zhenxi Zhang, Haoyue Tan, Xiaoran Shi, Yu Li, and Jiankun Ma are with the School of Electronic Engineering, Xidian University, Xi'an 710071, China (e-mail: xrshi@xidian.edu.cn).

Heng Zhou is with the School of Artificial Intelligence and Computer Science, Jiangnan University, Wuxi 214122, China.

Yun Lin is with Harbin Engineering University, Harbin 150009, China.

Xueru Bai is with the National Key Laboratory of Radar Signal Processing, Xidian University, Xi'an 710071, China.

Feng Zhou is with the School of Aerospace Space and Technology, Xidian University, Xi'an 710071, China.

Digital Object Identifier 10.1109/TCCN.2026.3657035

information about unknown modulation types during training, which poses significant challenges in distinguishing between known and unknown modulation types. In practical scenarios where test signals may come from the unknown modulation class, a conventional method to discriminate between known and unknown modulation types is setting a threshold on the SoftMax probability [12]. The assumption is that the model typically generates higher probabilities for known classes compared to unknown classes. However, when processing test samples from unknown classes, deep neural networks often demonstrate overconfident predictions [13]. A prevalent deep learning method [14], [15] for open set recognition first generates pseudo training data for unknown classes and then adds an extra output node to the final layer of the network to predict these unknown data. This method allows the network to maintain closed-set classification capability while simultaneously enabling unknown class recognition. Although this method performs well in computer vision, its effectiveness diminishes significantly in AMR, achieving only a 15.53% AUROC on the RML2016.10a dataset at an openness level of 20.94%. This limitation may stem from the inherent heterogeneity between communication signals and visual image data. In this paper, to make the model more forward-compatible for unknown modulation classes, we aim to endow the model with a 'future-proof' ability [16], which can accurately recognize the unknown modulation classes that may emerge in the future test time. Instead of generating pseudo new signals, we propose a modulation manifold mixup method [17] to fuse two feature embeddings from different classes and consider the fused embeddings as the virtual unknown modulation classes. Further, we enable the network to predict the virtual unknown class.

On the other hand, the traditional cross-entropy loss employed in AMR lacks explicit constraints on the feature space under open-set condition, resulting in minimal separation between clusters of known modulation types in the feature space. Consequently, the unknown signals resembling the known modulation types tend to overlap with these clusters, leading to poor performance on open-set recognition [10]. To address these limitations, many researchers have conducted preliminary investigations [10], [11]. Vaze et al. [18] suggest that simply applying better representation learning techniques to closed-set classifiers can significantly enhance their performance in OSR tasks. Motivated by this finding, Chen, et al. [10] employ triplet loss to constrain the sample-wise pairwise distances between different signals. Zhang, et al. [11] exploit the feature similarity from a sample-to-centroid perspective. However, existing feature space optimization methods for open-set recognition mainly emphasize inter-class separability, while neglecting other crucial factors including feature response differences between known and unknown classes, and intra-class compactness. For instance, pairwise distance loss cannot effectively constrain all class distinctions, thus restricting model generalization. Moreover, relying solely on sample-to-centroid similarity fails to capture local sample distance relationships.

This paper proposes a multi-level feature distribution constraint method which develops different granularity levels, global inter-sample relationships and local inner-sample activation patterns, in the representation space. We introduce a sample-centroid constraint to simultaneously enhance intra-class compactness within each modulation category and improve inter-class separation between different modulation types. Furthermore, we design an inner-sample level constraint, max-min feature constraint (MMFC), which operates on the feature vector activations, emphasizing local extreme responses and suppressing redundant activations, thus improving the inner-sample feature purity and enhancing the distinctiveness from the activation patterns of unknown modulation signals.

In conclusion, we design a novel method for AMOSR by designing multi-level feature distribution constraint method based on pseudo modulation placeholder method, termed multi-level feature distribution learning (MLFDL), as illustrated in Fig. 2. The detailed contributions of this paper are summarized as follows:

- We propose a novel pseudo-modulation generation method based on manifold mixup, which enables the model to better comprehend the concept of unknown modulation types while enhancing its forward compatibility for recognizing potential unknown modulated signals.
- We propose a sample-centroid contrastive learning method which enforces intra-class compactness and inter-class separability by aligning sample-level features with their corresponding class centroids.
- We propose an inner-sample level MMFC to explicitly enhance the divergence between the feature distributions of known and pseudo-novel signals, thereby strengthening the model's discrimination capability in open-set conditions.
- The proposed method utilizes minimum sample-to-centroid distances between sample features and class centroids for effective unknown modulation rejection. Comprehensive evaluations across multiple datasets show significant improvements in both AUROC and OSCR over state-of-the-art approaches, demonstrating MLFDL's superior effectiveness and generalization.

The rest of the paper is organized as follows: In Section II, we briefly introduce the related works. In Section III, we elaborate on the details of the proposed MLFDL method. In Section IV, we report and analyze the AMOSR results. Finally, in Section V, we conclude this work.

II. Related Work

A. Model-Driven Automatic Modulation Recognition

Traditional AMR algorithms can generally be categorized into two main types: likelyhood-based (LB) methods and feature-based (FB) methods [19]. LB methods [20], [21] calculate the likelihood function for the potential modulation types of the received symbol sequence, making decisions using a Bayesian or Neyman-Pearson hypothesis testing framework, such as, average likelihood ratio test or generalized likelihood ratio test. Although LB methods construct an optimal solution in the Bayesian sense, they suffer from poor robustness due to sensitivity to model mismatch and high

computational complexity. FB methods extract hand-crafted features of the signals, typically falling into three categories [22]: instantaneous features, statistical features, and transform-domain features. Specifically, instantaneous features describe the radio signal in terms of amplitude, frequency, and phase across various modulation types. Higher-order statistics [23] and cyclostationary moments [24] are widely used statistical characteristics to describe the periodic features. Then, the auto-correlation function and the spectral correlation are employed to facilitate the accurate classification of modulation types based on these features. However, the hand-crafted features often require domain expertise and have limited discriminative power in dynamic environments, making them with poor adaptability to varying channel conditions. Transform-domain analysis represents an effective signal processing technique, including wavelet transforms and random transforms [25]. Subsequent machine learning classifiers - such as support vector machines [25], neural networks [26], and decision trees [27] are typically applied to these transform-domain features for modulation classification. However, this conventional pipeline adopts two-stage architecture approach including feature extraction and separate classifier training. This two-stage approach introduces some fundamental limitations, including the increased system complexity due to independent optimization of two components, limited adaptability to new data distributions, and poor generalization across varying channel conditions.

B. Data-Driven Automatic Modulation Recognition

Deep learning (DL) methods [4], [28], [29] have gained significant attention in AMR owing to their powerful feature extraction capabilities and end-to-end learning framework. Typical DL-based approaches utilize CNN, LSTM, Transformer, or their hybrid architectures to automatically extract discriminative signal features for modulation classification. O'Shea et al. [28] pioneer CNN to extract the features of I/Q sequences, demonstrating the superiority of deep learning techniques in AMR. Wang et al. [4] design a modulation recognition CNN model, DrCNN, based on constellation diagrams, effectively improving the recognition of challenging modulations (e.g., QAM16/64), under low signal-to-noise ratio (SNR) conditions. In addition, the RNN structure has been explored for AMR by several studies [2], [5]. Rajendran et al. [5] implement LSTM models on resource-constrained sensors. In addition, Huang et al. [2] combine CNN with RNN to develop a convolutional long-short term deep neural network (CLDNN), achieving a notable enhancement in classification accuracy. While these studies highlight the importance of temporal feature extraction, RNN-based methods face computational efficiency challenges as their processing complexity grows linearly with signal length.

The transformer architecture, enhanced by its multi-head attention mechanism [30], excels at extracting global contextual information from signals. This capability enables effective modeling of long-range dependencies in signal data. Cai et al. [6] develop a specialized transformer network that leverages global signal information and semantic relationships to achieve robust classification under low SNR conditions.

Auto-encoders [31] represent an unsupervised learning framework comprising an encoder-decoder structure. The encoder maps input data to a low-dimensional latent space, while the decoder reconstructs the original input from this compressed representation. Ke and Vikalo [32] design an LSTM-based denoising autoencoder network that extracts noise-resistant features for modulation recognition. Ali et al. [33] combine I/Q constellation diagrams and higher-order cumulants as inputs, and design a two-layer sparse auto-encoder structure for modulation recognition.

However, these methods follow an inherent closed-set assumptions during training, mianly designed for known modulation categories. When faced with unknown modulation types in the test set, these methods confidently classify the unknown signals into the known modulation categories, failing to reject unknown modulation types. These shortcomings highlight the importance of developing AMOSR methods for practical deployment scenarios.

C. Automatic Modulation Open-Set Recognition

AMOSR aims to accurately classify known modulation types and reliably reject unknown modulation types. As shown in Fig. 1, current OSR methods fall into two categories, discriminative methods and generative methods.

Discriminative approaches for open-set recognition typically involve distinct strategies to discriminate unknown classes [34], such as analyzing SoftMax probability distributions [12], assessing prediction confidence via entropy measurements [35], or computing the distance between sample features and known class centroids [18], [36]. The OpenMax method [12] combines deep learning with extreme value theory to explicitly model unknown class likelihood. ARPL [36] aims to separate known and unknown distributions by identifying reciprocal points that represent inter-class differences. Recent advances [37], [38], [39] have focused on optimizing feature distributions for open-set conditions through contrastive learning [40]. For example, Xu et al. [37] exploit the supervised contrastive learning to enhance the feature distribution for open-set recognition. Kong, et al. [39] apply similar principles to maximize intra-class similarity and minimize inter-class similarity in jamming signal classification. These methods collectively advance the field by improving feature representation learning under open-set conditions.

The generative methods can be further divided into instance generation methods [14], [41] and non-instance generation methods [3], [42]. Instance generation methods employ generative models to synthesize unknown samples. For example, OpenGAN [14] uses GAN to generate negative features resembling unknown samples. Zhou et al. [41] employ manifold mixing to synthesize pseudo-novel classes, establishing placeholder representations that mitigate overconfidence in closed-set predictions while anticipating potential open-set data. Non-instance generation methods typically recognize unknown samples by analyzing reconstruction errors from trained auto-encoder models. For example, Huang et al. [42] develop class-wise auto-encoders to reconstruct semantic features extracted by the backbone network, with unknown-class

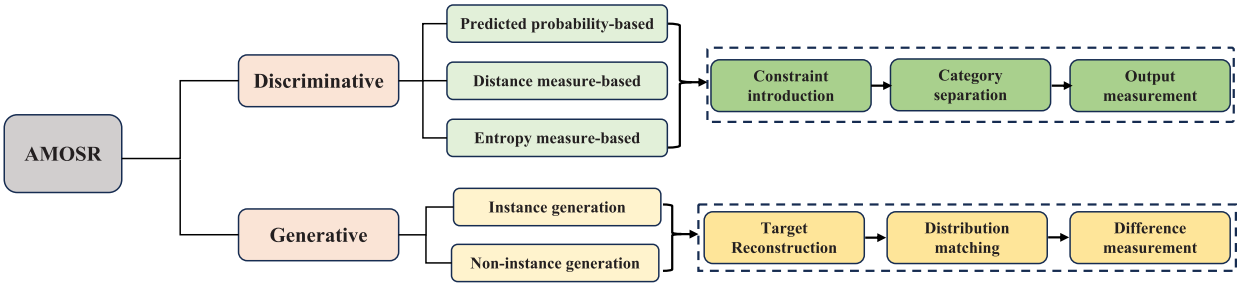

Fig. 1. The typical AMOSR methods can be divided into the discriminative methods and the generative methods.

samples exhibiting higher reconstruction errors than known categories.

However, these open-set recognition methods are primarily designed for image recognition and may not be fully applicable to signals. Compared to image recognition, the classification of signal modulation requires consideration of more abstract and complex features [43]. Moreover, the signals are often affected by various noise and interference, such as, white noise and multi-path effects, which substantially degrade feature representations and complicate recognition tasks. To address these challenges, the modified generalized end-to-end (GE2E) loss function [11] improves network training through adaptive thresholds and sample-to-centroid similarity optimization for AMOSR. OMR-DRL [10] utilizes the Otsu method to recognize the known and unknown modulation signals. While existing methods primarily improve open-set rejection through threshold optimization, they exhibit two critical limitations: inadequate consideration of implicit feature space organization, and failure to simultaneously achieve intra-class compactness for known modulations and sufficient feature space allocation for unknown types. These shortcomings fundamentally constrain the separability between known and unknown classes in the learned representation space. To overcome these limitations, we propose a novel AMOSR method that develops multi-level feature distribution constraints based on pseudo-novel modulation placeholder.

III. Methodology

A. Problem Definition

In dynamic open communication environments, the close-set trained model $f(\cdot)$ confronts test signals $\hat{\mathcal{D}}_{\text{te}} = \{(x_i, y_i)\}_{i=1}^{L}$ containing previously unseen modulation types, $y_i \in \hat{\mathcal{Y}} = \{1, \ldots, K, K+1\}$ represents the extended label space where class $K+1$ aggregates all unknown modulation types, potentially comprising multiple different modulation signals. The fundamental challenge lies in developing an AMOSR model capable of detecting this composite unknown class $K+1$ without prior exposure to any unknown signals during training. This problem can be formally expressed as an expected risk minimization [22] as:

$$f^* = \arg\min_{f \in \mathcal{H}} \mathbb{E}_{(x,y)\sim\hat{\mathcal{D}}_{\text{te}}} \mathbb{I}(y \neq f(x)) \tag{1}$$

where $f(\cdot)$ represents the AMOSR model, decoupled into a feature extractor $\phi(\cdot)$ and a linear classifier parameterized by W. In this paper, we employ MCLDNN [44] as the feature extractor as illustrated in the subplot (a) of Fig. 2. The complete training and testing procedure, outlined in Algorithm 1, integrates our novel contributions, a pseudo-modulation placeholder generation method and a multi-level feature distribution constraint framework.

Algorithm 1 MLFDL

Input: $\mathcal{D}_{\text{tr}} = \{(x_i, y_i)\}_{i=1}^{N}$, the feature extractor $\phi(\cdot)$, the linear classifier W, the test signal sample x_{ti}.

Output: the trained AMOSR model $\hat{f}(\cdot)$, the open-set modulation classification result $\hat{y}_{ti}$.

Pseudo Novel Modulation Placeholder:

(1) Generate the feature embeddings of known signals by Eq. 2;

(2) Generate the pseudo novel modulation placeholders using Eq. 3;

(3) Introduce the modulation classification loss $\mathcal{L}_{MC}$ by Eq. 4.

Multi-level Feature Distribution Constraint:

Sample-centroid Contrastive Learning:

(1) Generate centroids using Eq. 7;

(2) Construct the positive pairs and negative pairs;

(3) Introduce the sample-centroid contrastive learning loss $\mathcal{L}_{CL}$ as Eq. 8.

Sample-wise Max-Min Feature Constraint:

(1) Calculate maximum and minimized feature value using Eq. 9 and Eq. 10, respectively;

(2) Introduce the max-min feature constraint as Eq. 11.

Overall Training:

(1) Train the AMOSR network $f(\cdot)$ according to Eq. 12.

Unknown rejection:

(1) Calculate the minimum distance to all centroids by Eq. 13;

(2) Calculate the average distance and set a rejection threshold th by Eq. 14;

(3) Execute the AMOSR using Eq. 15.

B. Network Architecture

The network employed in this paper comprises three core components: Multi-channel Feature Extraction, Temporal Feature Modeling, and FC Classifier. As depicted in Fig. 2 (a), the processing pipeline begins with multi-channel feature extraction where I-channel, Q-channel, and combined I/Q

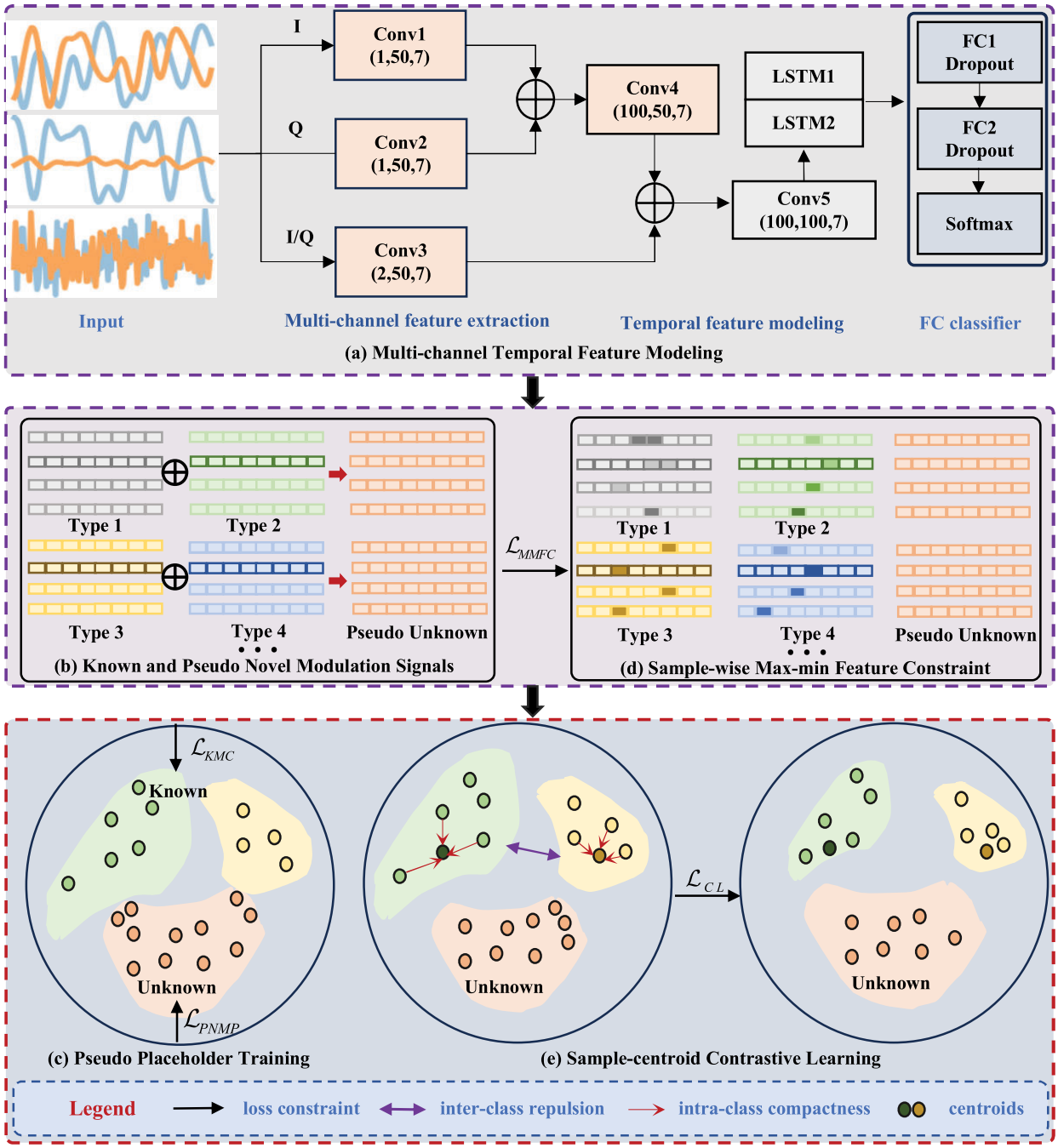

Fig. 2. The flowchart of the proposed MLFDL. (a) We employ multi-channel temporal modeling method to extract features. (b) We generate the pseudo unknown modulation signals. (c) We introduce the pseudo placeholder training. (d) We propose a sample-wise max-min feature constraint. (e) We develop a sample-centroid contrastive learning method.

signals are independently processed through three parallel 1D CNNs, conv1, conv2, and conv3. The extracted I-channel and Q-channel features are then concatenated and further processed by conv4, before being fused with the I/Q-channel features from conv3 to form a comprehensive multi-channel representation. These features subsequently undergo temporal modeling through conv5 and two LSTM networks, each with 128 cells, to capture sequential dependencies in the signal data. The multi-channel feature extraction and temporal feature modeling are used to extract features for contrastive learning. The positive sample pairs are constructed between signal features and their corresponding class prototypes, while the negative pairs are formed using centroids of other modulation types, with all features maintaining a consistent 128-dimensional representation after two LSTM networks. Finally, the architecture employs two fully connected layers followed by a Softmax layer to perform the final modulation classification.

C. Pseudo Novel Modulation Placeholder

In AMOSR task, the objective is to reject all unknown-class signals. However, some unknown signals share similar

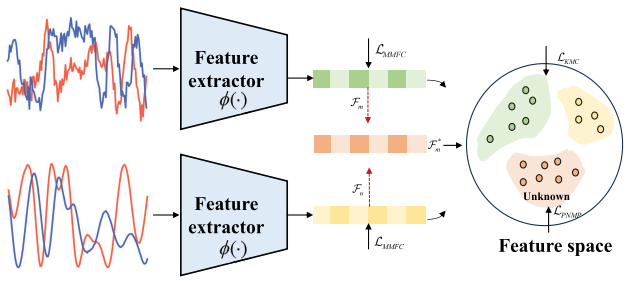

Fig. 3. The schematic diagram of the proposed pseudo novel modulation placeholder method. The red dashed arrow represents the mix-up operation.

properties with known signals, resulting in feature-space overlap that may lead to rejection failures. To address the dual challenges of calibrating closed-set classifiers while preserving sufficient feature space for unknown modulation types, we propose a pseudo novel modulation placeholder (PNMP) method which leverages manifold mixup to simulate these hard pseudo-unknown samples located in regions of high similarity, which are difficult to distinguish from known signals. The PNMP method incorporates novel modulation generation with pseudo open-set training. In addition, for the fidelity of OOD samples, although the mixup-generated signals are not intended to directly simulate these signals that exhibit significant distributional divergence from known classes, when these unknown signals enter the model, their feature representations usually lie at a sufficiently large distance from the centroids of known classes. Consequently, our model can effectively reject these samples based on the sample to centroids distances.

For computation complexity, the traditional methods relying on generative models to simulate new modulation types face significant limitations, including the inherent difficulty in accurately modeling unknown signal distributions and the substantial computational burden of model retraining. In contrast, the effective unknown signal placeholders generated by PNMP exhibit different distributional characteristics compared to known classes while maintaining computational efficiency, which overcomes these limitations and provides an efficient mechanism to anticipate novel modulation signals. Specifically, given two samples x_m and x_n with distinct labels, the feature embeddings of x_m and x_n are extracted by the feature extractor $\phi(\cdot)$, denoted as $\mathcal{F}_m \in \mathbb{R}^D$ and $\mathcal{F}_n \in \mathbb{R}^D$, respectively.

$$\mathcal{F}_m = \phi(x_m), \mathcal{F}_n = \phi(x_n) \tag{2}$$

We employ the manifold mixup operation as shown in Fig. 3:

$$\mathcal{F}_m^* = \lambda \mathcal{F}_m + (1-\lambda)\mathcal{F}_n, y_m \neq y_n \tag{3}$$

Our approach generates these combinations within mini-batches during training. Given a batch size B, we randomly select $B/2$ pairs of samples from different modulation classes and apply manifold mixup to create synthetic representations. This strategy specifically addresses the critical challenge posed by unknown modulation signals that exhibit high similarity to known types. To enhance the model discriminative capability for these borderline cases, we sample the mixup coefficient λ from the constrained interval $[0.98, 1)$, deliberately generating pseudo-novel modulation placeholders that closely resemble known classes. This controlled approach serves the purpose of strengthening the model's ability to recognize ambiguous unknown modulation features while maintaining adequate feature space allocation around known-class clusters. By focusing on this sampling range, we effectively reserve feature space for potentially similar unknown modulation types while preserving clear decision boundaries between known and unknown categories.

Consequently, we define the embedding $\mathcal{F}_m^*$ as pseudo-open-set modulation types, assigning them the novel class label $K+1$ during training. The model processes both the original training signals and these synthesized exemplars through the classification layer, where $W \in \mathbb{R}^{(K+1)\times D}$ parameterizes the weight matrix for final prediction. This formulation naturally decomposes the modulation classification loss $\mathcal{L}_{MC}$ into two distinct components, the known modulation classification loss $\mathcal{L}_{KMC}$ and the pseudo-novel modulation placeholder loss $\mathcal{L}_{PNMP}$:

$$\mathcal{L}_{MC} = \mathcal{L}_{KMC} + \mathcal{L}_{PNMP} \tag{4}$$

For the known modulation types, $\mathcal{L}_{KMC}$ is formulated as:

$$\mathcal{L}_{KMC} = \frac{1}{N}\sum_{i=1}^{N} \ell(f(x_i), y_i) \tag{5}$$

which $\ell()$ denotes the standard cross-entropy loss function. For the augmented pseudo-samples $\mathcal{F}^*$, the pseudo-novel modulation placeholder loss $\mathcal{L}_{PNMP}$ is defined as:

$$\mathcal{L}_{PNMP} = \ell(W^T \cdot \mathcal{F}^*, K+1) \tag{6}$$

D. Multi-Level Feature Distribution Constraint

This subsection details the proposed multi-level feature distribution constraint (MFDC) method, incorporating both sample-centroid contrastive learning and sample-wise MMFC. The contrastive learning method employs a specialized loss function to promote intra-class compactness and inter-class separability by mapping sample-level features to their corresponding class centroids. Meanwhile, the MMFC explicitly enhances the feature distribution divergence between known and unknown signals. These constraints collaboratively optimize the model feature representation for open-set scenarios, improving its ability to reject unknown modulation types.

1) Sample-Centroid Contrastive Learning: We aggregate the feature representation of the training signals $\mathcal{F} \in \mathbb{R}^{N\times D}$ in the current training epoch by the feature extractor, where N and D represent the number of training signals and feature dimension, respectively. Given the true modulation label y_i, we generate the centroid vector $\mathcal{C}_k \in \mathbb{R}^D$ of the modulation type k as follows:

$$\mathcal{C}_k = \frac{\sum_{i=1}^{N} \mathcal{F}_i \cdot \mathbb{1}\left[y_i = k\right]}{\sum_{i=1}^{N} \mathbb{1}\left[y_i = k\right]} \tag{7}$$

where i is the sample index, $\mathcal{F}_i \in \mathbb{R}^D$ is the feature representation of sample i. To generate more compact intra-class feature distribution and more separable inter-class clusters, as illustrated in Fig. 4, we propose a sample-TO-centroid contrastive learning method that encourages the feature representation of

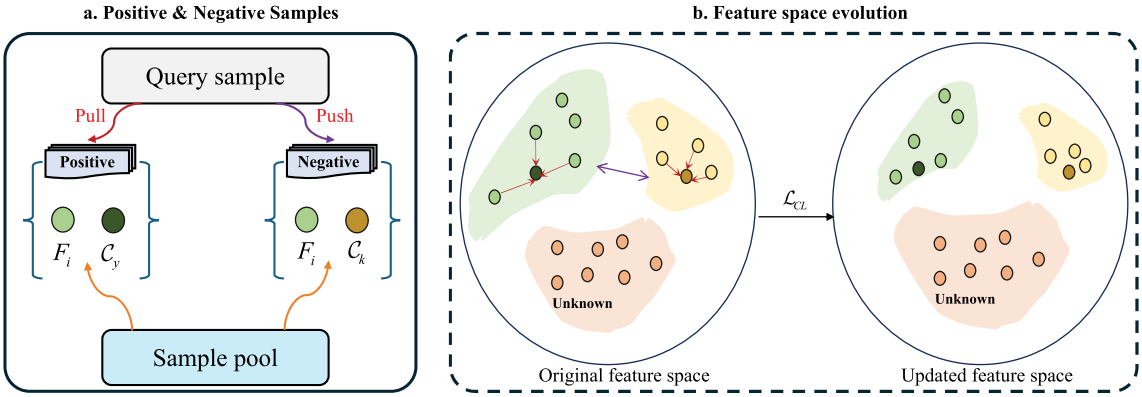

Fig. 4. Subplot (a) denotes the construction process of positive and negative samples in sample-centroid contrastive learning. Subplot (b) denotes the feature space evolution with contrastive learning method.

an anchored sample $\mathcal{F}_i$ to align closely with its associated cluster centroid $\mathcal{C}_y$ based on its ground-truth label y, while simultaneously driving $\mathcal{F}_i$ away from the centroids of all other classes. This process is optimized by $\mathcal{L}_{CL}$ as follows:

$$\mathcal{L}_{CL} = -\log \frac{\exp\left(Norm(\mathcal{F}_i) \cdot Norm(\mathcal{C}_y)/\tau\right)}{\sum_{k=1}^{K} \exp\left(Norm(\mathcal{F}_i) \cdot Norm(\mathcal{C}_k)/\tau\right)} \tag{8}$$

where $Norm$ denotes the l_2 normalization operation of the feature vector and τ is the temperature parameter, which is set to 0.1 empirically. The contrastive learning aims to ensure the feature space with smaller intra-class distances and larger inter-class separations, thereby leaving sufficient feature space for potential unknown classes. $\mathcal{F}_i$ and $\mathcal{C}_y$ constitute the positive pair. $\mathcal{F}_i$ and the centroid vectors of other classes form the negative pairs in contrastive learning. In addition, the red arrows represent the pull operation between positive samples, while the purple arrows indicate the push operation between negative samples. Through the introduction of the contrastive loss term $\mathcal{L}_{CL}$, the model optimizes its feature geometry to maintain reserved compatibility regions for unknown modulation types, thereby mitigating open-space risk.

2) Sample-Wise Max-Min Feature Constraint: Building upon the fundamental divergence in feature representation properties between known and unknown signals, we propose a MMFC method to enhance discriminative feature learning for known modulation types while improving detection capability for open-set signals. The underlying principle stems from the observation that well-trained models naturally develop distinct activation patterns: known-class signals exhibit prominent features with high activation magnitudes corresponding to class-discriminative characteristics alongside suppressed features with minimal magnitudes, whereas unknown signals demonstrate uniformly attenuated activation profiles due to their absence during training. To systematically enforce this discriminative structure, our MMFC implements simultaneous constraints on feature magnitudes by maximizing salient activations for known-class patterns while minimizing non-discriminative responses. The implementation begins by identifying the most significant feature dimension per sample through:

$$\mathcal{F}_{imax} = \max_{1 \le j \le D} \left|\mathcal{F}_{ij}\right| \tag{9}$$

where j denotes the j^{th} element in the feature embedding $\mathcal{F}_i$. Then, we define the minimized feature value of each sample as:

$$\mathcal{F}_{imin} = \min_{1 \le j \le D} \left|\mathcal{F}_{ij}\right| \tag{10}$$

Therefore, the proposed MMFC is optimized by $\mathcal{L}_{MMFC}$ as:

$$\mathcal{L}_{MMFC} = \mathcal{F}_{imin} - \mathcal{F}_{imax} \tag{11}$$

This constraint amplifies discriminative feature responses for known classes while maintaining subdued activations for non-characteristic features, thereby sharpening the separation between known and unknown modulation types in the feature space.

E. Training Phase and Test Phase for MLFDL

The overall training loss for the proposed MLFDL method consists of three parts, the modulation classification loss $\mathcal{L}_{MC}$, the sample-centroid contrastive loss $\mathcal{L}_{CL}$, and the sample-wise max-min feature constraint $\mathcal{L}_{MMFC}$, which is formulated as:

$$\mathcal{L}_{MLFDL} = \mathcal{L}_{MC} + \lambda_{CL}\mathcal{L}_{CL} + \lambda_{MMFC}\mathcal{L}_{MMFC} \tag{12}$$

where λ_{CL} and λ_{MMFC} are used to adjust the contribution of sample-centroid contrastive learning and sample-wise MMFC.

In the test stage, we feed the test signal x_t into the network to get its corresponding feature embedding $\mathcal{F}_t$. Then, we calculate the minimum distance from $\mathcal{F}_{ti}$ to all known modulation centroids $\mathcal{C}_k$, denoted as dis_{ti}:

$$dis_{ti} = \min_{1 \le k \le K} \|\mathcal{F}_{ti} - \mathcal{C}_k\|_2 \tag{13}$$

Then, we calculate the average distance dis_{avg} of all test samples and set a rejection threshold th following Eq. 14:

$$dis_{avg} = \frac{1}{N}\sum_{i=1}^{L} dis_{ti},\ th = \beta \cdot dis_{avg} \tag{14}$$

where β is set to 1.2 empirically. If dis_{ti} of a test sample is greater than th, it is rejected as an unknown modulation signal with the label of $K+1$, which is formulated as:

$$\hat{y}_{ti} = \begin{cases} \underset{k=1,\cdots,K}{\operatorname{argmax}} \boldsymbol{w}_k^{\top}\phi(x_{ti}) & dis_{ti} < th \\ K+1 & \text{otherwise} \end{cases} \tag{15}$$

The predictions less than *th* are classified as the corresponding known modulation type.

IV. Experiments

A. Evaluation Metric and Implementation Details

Following [36], [45], we use the Area Under Receiver Operating Characteristic (AUROC) curve to evaluate the AMOSR performance on both known and unknown test signals. The AUROC metric assesses the discrimination ability between known and unknown signals, with a value closer to 1 indicating better open-set recognition performance. Notably, AUROC does not require setting specific thresholds for comparison. However, while AUROC effectively distinguishes between known and unknown modulation types in probability distributions, it does not assess the model prediction accuracy for known classes. To address this limitation, we additionally employ the open-set classification rate (OSCR) metric as proposed in [18], which incorporates both the rejection rate of unknown classes and the accuracy of known classes.

In addition, we use accuracy on known samples (AKS), accuracy on unknown samples (AUS), and normalized accuracy (NA) to evaluate the performance of the AMOSR models comprehensively. AKS denotes the probability of correctly classifying known modulation signals, whereas AUS represents that the probability of an unknown sample is correctly recognized by the model. The formulas of AKS is defined as follows:

$$AKS = \frac{\sum_{i=1}^{K} T_i K_i}{\sum_{i=1}^{K} \left(T_i K_i + \sum_{i=1, j \neq i}^{K} F_i K_j \right)} \tag{16}$$

$T_i K_i$ denotes denote the number of correctly classified samples from known class i. $F_i K_j$ represents the number of known-class samples with true label j that are misclassified as class i. For unknown signal recognition, we define TU as the number of correctly rejected unknown-class samples, FU as the number of unknown-class samples incorrectly predicted as known classes. The formula of AUS is defined as:

$$AUS = \frac{TU}{TU + FU} \tag{17}$$

The NA metric is derived through a combination of AKS and AUS, providing a balanced evaluation of both known-class classification and open-set rejection performance, which is formulated as:

$$NA = \lambda_r AKS + (1 - \lambda_r) AUS \tag{18}$$

where λ_r is set as the ratio of known modulation types to the total number of modulation categories.

As shown in Table I, we use the RML2016.10a [28] dataset and RML2016.10b dataset [46] to evaluate the AMOSR performance, which are widely used in AMR. The RML2016.10a dataset consists of 11 modulation types, 8 digital types and 3 analog types. The 8 digital modulations are BPSK, QPSK, 8PSK, 16QAM, 64QAM, BFSK, CPFSK, and PAM4, and 3 analog modulations are WBFM, AM-SSB, and AM-DSB. The RML2016.10b dataset encompasses WBFM, QPSK, 64QAM, 16QAM, PAM4, GFSK, CPFSK, BPSK, AM-DSB, and 8PSK.

TABLE I
Detail Parameters of Datasets

Dataset	**RML2016.10a**	**RML2016.10b**
Modulation number	11	10
Total number of samples	220000	1200000
Signal size	2×128	2×128
SNR range	-20:2:18dB	-20:2:18dB

The SNR ranges from −20 dB to 18 dB, with an interval of 2, and the length of each sample is 128. The RML2016.10a dataset contains 1000 signals for each modulation and SNR combination, 220,000 signals in total. As shown in Table II, we set two different openness levels, specifically 20.94% and 5.13%. Under the 20.94% openness condition, there are 5 known modulation types and 6 unknown modulation types. Under the 5.13% openness condition, there are 9 known modulation types and 2 unknown modulation types. The RML2016.10b dataset has 6000 signals of each modulation and SNR combination, 1200000 signals in total. As shown in Table II, we also set two different openness levels, specifically 18.35% and 9.25%. Under the 18.35% openness condition, there are 5 known modulation types and 5 unknown modulation types. Under the 9.25% openness condition, there are 7 known modulation types and 3 unknown modulation types. The training-validation-testing ratio for both datasets is 6:2:2. The framework is implemented in PyTorch with a NVIDIA GeForce RTX 4090 GPU. We adopt the Adam optimizer in the training procedure. The learning rate is set to 0.002. The total training iteration is set to 1000. All models are built on Python 3.8 in PyTorch 2.0.1.

B. Comparison With Other AMOSR Methods

We compare the proposed framework with other existing competitive open-set modulation recognition method, SoftMax, OpenMax [12], GCPL [47], RPL [45], ARPL [36], OMR-DRL [10], GE2E [11], and PROSER [41]. Note that all groups use the same data augmentation methods, training strategies, and backbone model for fair comparisons.

1) AMOSR Performance on RML2016.10a Dataset: As illustrated in Table I, we set 9 modulation types and 2 modulation types as the known class and unknown class, respectively, on RML 2016.10a dataset. We test the AMOSR performance of different methods when SNR belongs to $[-10\text{dB}, 18\text{dB}]$ with a step of 2dB. We provide the average AMOSR performance when openness is 5.13% and 20.94% in Table III and Table IV, respectively.

As shown in Table III, the proposed MLFDL achieves consistently superior results on AUROC, OSCR, AKS, AUS, and NA, respectively on RML2016.10a dataset when the openness is 5.13%. In this configuration, the number of unknown classes is 2. Specifically, our method achieves a significant improvement of 10.39% on AUROC compared the second-best method OMR-DRL. In addition, MLFDL outperforms the second-best PROSER on OSCR by 7.44%. As illustrated in Table IV, our method achieves the best OSCR of 85.39% and the best AUROC of 96.30% when openness is 20.94% with

TABLE II
EXPERIMENTAL SETTINGS WITH DIFFERENT DEGREES OF OPENNESS

Dataset	Openness	Known classes	Unknown classes
RML2016.10a	5.13%	AM-SSB, BPSK, CPFSK, GFSK, PAM4, QPSK, 8PSK, QAM16, QAM64	WBFM, AM-DSB
	20.94%	AM-SSB, BPSK, CPFSK, GFSK, PAM4	QPSK, 8PSK, QAM64, QAM16, WBFM, AM-DSB
RML2016.10b	9.25%	QPSK, WBFM, CPFSK, GFSK, PAM4, QAM16, QAM64	8PSK, BPSK, AM-DSB
	18.35%	8PSK, BPSK, CPFSK, GFSK, PAM4	QAM16, QAM64, QPSK, WBFM, AM-DSB

TABLE III
THE AVERAGE AMOSR PERFORMANCE (%) ON RML2016.10A DATASET WHEN SNR BELONGS TO [−10dB, 18dB] WITH A STEP OF 2DB AND THE OPENNESS IS 5.13%

Method	AUROC	OSCR	AKS	AUS	NA
SoftMax	61.61	56.74	55.72	46.10	53.97
GCPL [47]	61.48	55.09	56.93	52.88	56.19
RPL [45]	49.17	43.72	46.21	43.41	45.70
ARPL [36]	48.20	42.52	44.64	41.72	44.11
OpenMax [12]	57.41	49.47	80.26	38.82	73.78
GE2E [11]	73.68	64.78	71.08	69.82	70.85
OMR-DRL [10]	77.80	65.30	64.36	66.91	64.82
PROSER [41]	72.35	67.78	73.23	64.66	71.67
MLFDL (Ours)	**88.19**	**75.22**	**81.55**	**77.17**	**79.70**

TABLE IV
THE AVERAGE AMOSR PERFORMANCE (%) ON RML2016.10A DATASET WHEN SNR BELONGS TO [−10dB, 18dB] WITH A STEP OF 2DB AND THE OPENNESS IS 20.94%

Method	AUROC	OSCR	AKS	AUS	NA
SoftMax	69.24	65.08	59.42	57.32	58.27
GCPL [47]	65.54	53.73	65.32	64.12	64.66
RPL [45]	66.12	61.30	67.70	65.49	66.49
ARPL [36]	50.51	47.23	49.23	45.28	47.07
OpenMax [12]	59.32	51.23	76.48	45.24	59.44
GE2E [11]	75.38	66.42	74.28	70.25	72.08
OMR-DRL [10]	82.32	75.54	80.12	77.43	78.65
PROSER [41]	73.56	65.31	75.67	67.55	71.24
MLFDL (Ours)	**96.30**	**85.39**	**95.37**	**88.99**	**91.79**

TABLE V
THE AVERAGE AMOSR PERFORMANCE (%) ON RML2016.10B DATASET WHEN SNR BELONGS TO [−10dB, 18dB] WITH A STEP OF 2DB AND THE OPENNESS IS 9.25%

Method	AUROC	OSCR	AKS	AUS	NA
SoftMax	60.12	52.43	69.12	23.38	55.39
GCPL [47]	68.12	62.32	76.31	40.34	65.52
RPL [45]	61.25	59.32	75.17	24.22	59.88
ARPL [36]	70.21	65.12	74.34	34.23	62.31
OpenMax [12]	58.26	56.34	85.34	25.32	67.33
GE2E [11]	68.23	59.12	90.12	30.24	72.16
OMR-DRL [10]	70.02	64.64	76.12	48.44	67.82
PROSER [41]	71.86	66.87	72.15	63.45	69.54
MLFDL (Ours)	**94.86**	**83.46**	**95.42**	**94.89**	**94.80**

TABLE VI
THE AVERAGE AMOSR PERFORMANCE (%) ON RML2016.10B DATASET WHEN SNR BELONGS TO [−10dB, 18dB] WITH A STEP OF 2DB AND THE OPENNESS IS 18.35%

Method	AUROC	OSCR	AKS	AUS	NA
SoftMax	55.10	50.18	81.79	18.78	50.29
GCPL [47]	64.09	61.32	77.93	45.50	61.72
RPL [45]	54.67	56.48	77.14	36.87	57.01
ARPL [36]	66.91	64.51	79.50	39.57	59.54
OpenMax [12]	65.55	59.54	88.43	21.31	54.87
GE2E [11]	67.10	50.16	80.81	37.96	59.38
OMR-DRL [10]	68.90	63.11	79.14	45.92	62.53
PROSER [41]	72.67	68.21	72.94	66.75	69.84
MLFDL (Ours)	**92.42**	**86.78**	**96.45**	**86.77**	**91.61**

6 unknown modulation types, demonstrating that our method can effectively reject the unknown modulation types while maintaining the classification capability for known modulation types with different known and unknown partitioning. This proves that the optimization based on PNMP and multi-level feature distribution constraint enhances the margin between the known and unknown modulation types in the feature space, preserving the inter-class separation of known modulation types. Furthermore, our method achieves the highest AKS and AUS among all compared methods, consequently attaining the highest NA of 91.79%. These observations validate that the adaptive threshold, *th*, based on the average distance metric, can not only maintain the recognition accuracy of known modulation types but also effectively reject unknown modulation types, thereby contributing to the stability of AKS and promoting the improvement of unknown-class sensitivity of AUS. These experimental results effectively demonstrate that our method achieves stable and favorable AMOSR performance across different numbers of unknown classes.

2) AMOSR Performance on RML2016.10b Dataset: Similarly, we conduct the comparative experiments for the AMOSR task on the RML2016.10b dataset to 8 competitive methods. We employ two different openness levels of 9.25% and 18.35%, respectively, with the SNR range from -10dB to 18dB and a step size of 2dB. In Table V, we present the average AMOSR performance across all experimental groups when the openness is 9.25%. MLFDL achieves the best AUROC and OSCR when the number of known classes is 7 and the number of unknown classes is 3 on RML2016.10b dataset. In terms of AUROC, our method outperforms the second-best approach, PROSER, by 23.00%. In terms of OSCR, our method achieves an 18.34% improvement compared to ARPL. In addition, MLFDL achieves a remarkable AUS of 94.89%, significantly outperforming other benchmark methods. These findings verify that the proposed MLFDL demonstrates consistent robustness in distinguishing known versus unknown signal categories under different dataset evaluation scenarios, while demonstrating robust resilience against performance degradation when encountering previously unseen modulation types.

As shown in Table VI, our method achieves consistently superior performance on AUROC, OSCR, AUS, and NA, respectively, when the openness is 18.35%. Specifically, our method outperforms the second-best PROSER by 19.75%

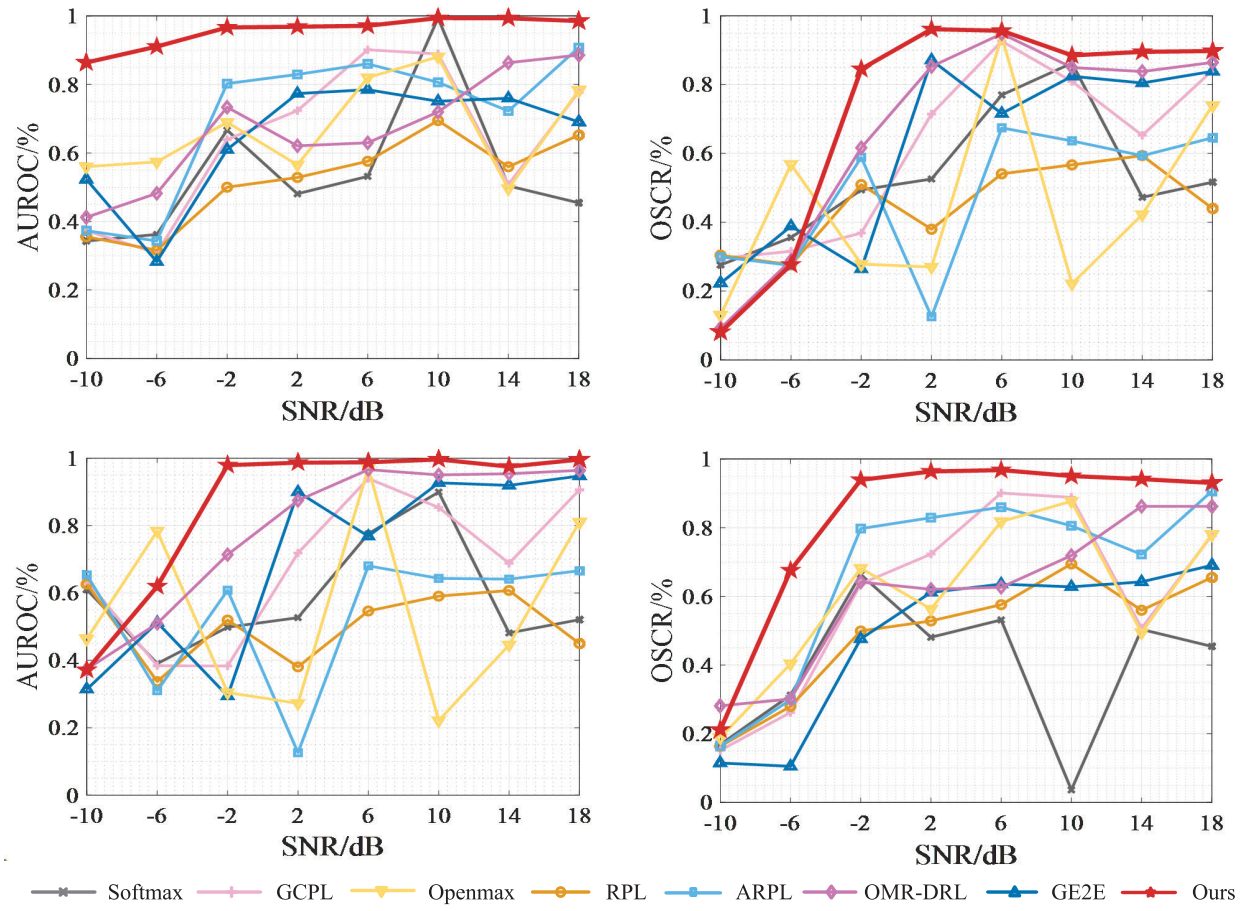

Fig. 5. The first row denotes the AUROC and OSCR results on RML.2016.10a dataset when openness is 5.13%. The second row denotes the AUROC and OSCR results on RML.2016.10b dataset when the openness is 18.35%.

on AUROC. In addition, our method gains an improvement of 18.57% on OSCR compared to PROSER. These findings demonstrate that under the condition of higher openness, our method maintains the distinctiveness between known modulation types and unknown modulation types. As for AKS and AUS, our method achieves the best average results of 96.45% and 86.77%, which verifies that our method effectively optimizes the empirical risk for known classes while simultaneously mitigating the open-space risk associated with unknown modulation types. The advantage of our method lies in the fact that our method enables the balance between the modulation recognition of known types and unknown types, achieving a best NA of 91.61% among all comparative methods. These results further support that the pseudo-novel modulation placeholder and multi-level feature distribution constraint proposed in this paper effectively optimize the feature space for AMOSR, facilitating a synergetic optimization of open-space risk and empirical risk.

As shown in Fig. 5, the performance of comparative methods fluctuates significantly with changes in SNR. The proposed method remains relatively stable. The relative stability of our method across different SNR conditions can be attributed to the optimized open-set feature space by our proposed components, which is fundamentally different from the comparative methods. Previous AMOSR methods lack mechanisms that explicitly encourage separation between known and unknown modulated signals, causing their feature distributions to collapse or overlap as noise levels increase, thereby leading to performance fluctuations. In contrast, our method establishes an open-set representation space through the following designs: (1) The proposed pseudo-modulation generation based on manifold mixup expands the feature manifold toward unknown regions, enabling the model to better internalize the concept of unseen modulation types and improving its rejection capability under noisy conditions. (2) The sample-centroid contrastive learning module enhances intra-class compactness and inter-class separability, making known-class clusters more robust against SNR degradation. and (3) The inner-sample MMFC further amplifies the divergence between known and pseudo-novel feature distributions, ensuring a clear decision boundary even when noise increases. These components yield a feature space inherently suitable for unknown rejection, resulting in stable performance across varying SNR levels, an advantage that comparative methods do not possess.

3) Complexity Analysis: Our work primarily compares different open-set recognition methods while keeping the modulation recognition model consistent across experiments. Taking the RML2016b dataset as an example, the training of 100 epochs requires 14.56 minutes, and the training time of

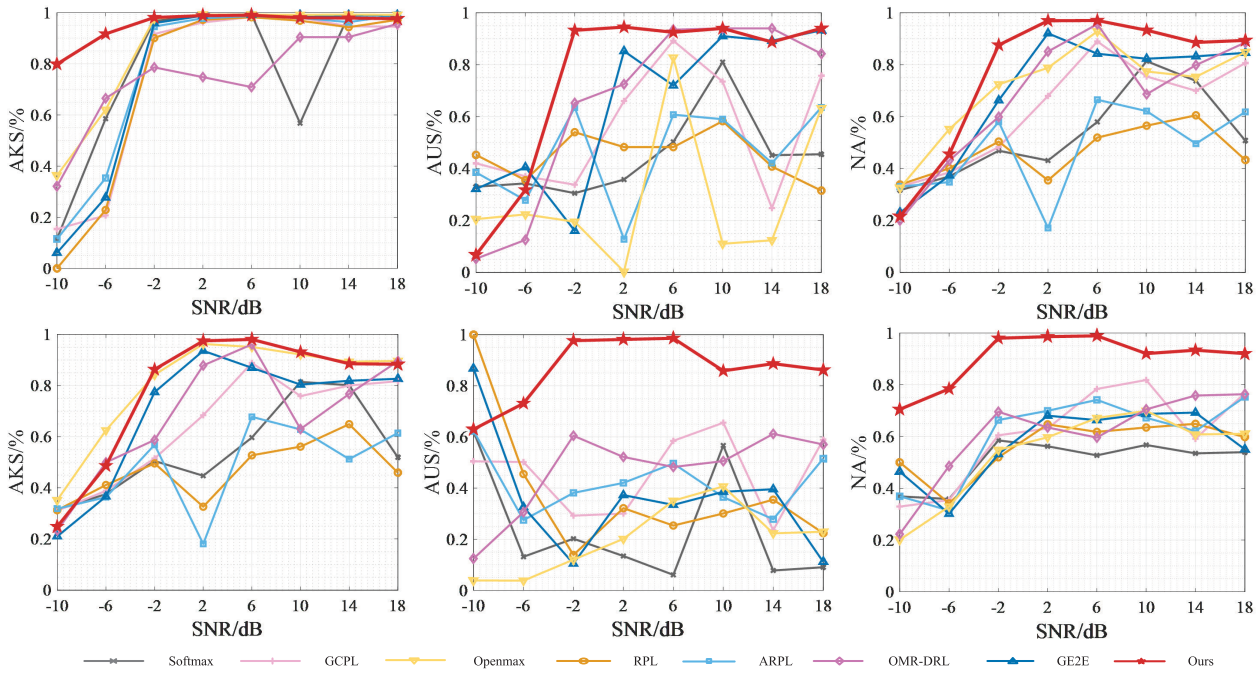

Fig. 6. The first row denotes the AKS, AUS, and NA results on RML.2016.10a dataset when openness is 5.13%. The second row denotes the AKS, AUS, and NA results on RML.2016.10b dataset when the openness is 18.35%.

TABLE VII
THE TRAINING TIME AND INFERENCE TIME OF DIFFERENT MODELS

Method	Training time (min)	Inference time (ms)
SoftMax	14.31	1.14
GCPL [47]	14.54	1.26
RPL [45]	14.55	1.27
ARPL [36]	14.53	1.32
OpenMax [12]	14.31	2512.43
GE2E [11]	14.46	4.52
ORM-DRL [10]	14.58	2511.32
PROSER [41]	15.89	5.14
MLFDL (Ours)	14.56	3.42

different methods remains almost identical under the same computational environment, as shown in Table VII. However, in the open-set recognition phase, a significant gap appears in inference efficiency. Methods such as OpenMax and ORM-DRL involve additional Weibull distribution fitting, which substantially increases their inference latency to the order of seconds, over 2500 ms per sample. In contrast, our proposed MLFDL method determines the rejection of unknown classes by computing the minimum distance between sample features and the centroids of known modulation types, and then comparing it with the average intra-class distance. This rejection mechanism allows our approach to maintain stable online inference within 10 ms per sample, with an average inference time of 3.42ms. Such results demonstrate that our method not only ensures competitive open-set recognition accuracy but also achieves a favorable trade-off between effectiveness and efficiency, thereby exhibiting promising feasibility for practical deployment.

C. Ablation Study

1) AMOSR Performance Under Different SNR Levels: We list the AUROC and OSCR performance across different datasets under various SNR levels in Fig. 5. In addition, we report AKS, AUS, and NA results different datasets under various SNR levels in Fig. 6. On RML2016.10a dataset, our method achieves consistent and stable growth on AUROC as SNR ranges from -10dB to 14dB in first subplot of the first row in Fig. 5. In contrast, other methods exhibit unstable unknown signal discrimination performance under different SNR levels as shown in the AUROC subplot of Fig. 5. In addition, as illustrated in the second subplot of the first row in Fig. 5, when SNR is greater than −2dB, our method achieves the best OSCR, which validates that the proposed method can maintain its recognition capability for known modulation types while effectively rejecting unknown ones. As SNR ranges from 6 to 18 dB, the comparative methods misclassify some known-class modulation signals as unknown-class modulation signals, accompanied by the issue of overfitting to the known-class training set, which results in a decline in classification accuracy for certain known-class signals during testing, as illustrated in the AKS subplot of Fig. 6. The fluctuated AKS value leads to reduction and fluctuation in OSCR, which comprehensively reflects the AMR accuracy of both known and unknown modulated signals. Compared to other methods, the proposed method achieves superior NA performance under different SNR levels. Moreover, the AKS attains above 90.00% even when unknown classes are introduced, demonstrating the effectiveness of our method in maintaining robust AMR performance on known modulation categories under open-set conditions. In terms of AUS, our method demonstrates stable performance, with significant advantages at −2dB and 2dB. Additionally, OMR-DRL achieves relatively high AUS at 14dB. On NA, our method consistently achieves superior performance at SNR levels above −2 dB, highlighting the effectiveness of the proposed PNMP and MFDC designs

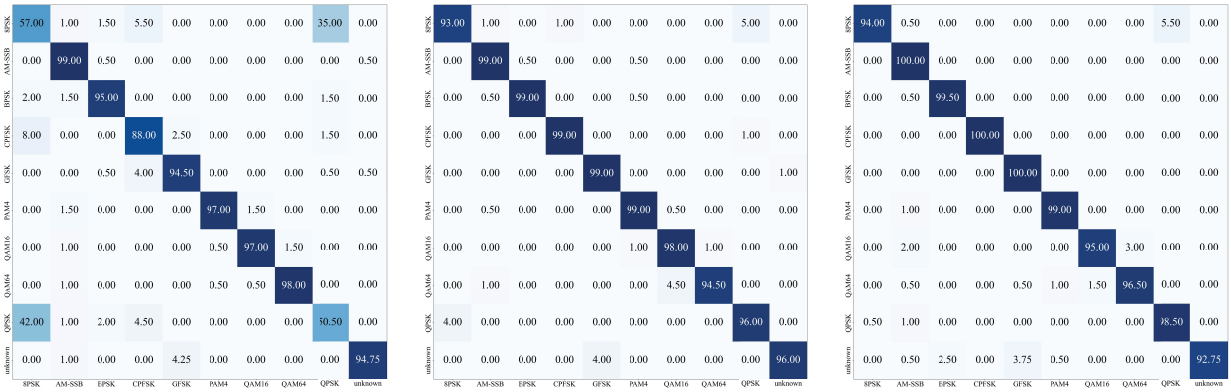

(a) (b) (c)

Fig. 7. Confusion matrices on RML2016.10a for different SNR levels. (a) SNR = −2dB. (b) SNR = 2dB. (c) SNR = 6dB. The vertical axis represents the true label, and the horizontal axis represents the predicted label.

for AMOSR. These results demonstrate that our approach provides strong discriminative capability in distinguishing between known and unknown modulation types.

As depicted in the second row of Fig. 5, on the RML2016.10b dataset, our method demonstrates substantial improvements in terms of AUROC and OSCR when the SNR exceeds −2dB compared with other methods, demonstrating balanced and stable performance in accurately classifying known modulation types while reliably detecting unknown ones. As shown in the second row of Fig. 6, in terms of AKS, OpenMax and GE2E exhibit competitive performance. However, these methods demonstrate limited effectiveness in rejecting unknown modulation types, with the classification performance degradation clearly observable in subplots (g) and (h). In contrast, our method significantly leads in terms of the AUS metric for rejecting unknown types while effectively recognizing known modulation types when the SNR is above −2dB. Ultimately, our method exhibits substantial and evident improvements in the NA metric. These findings further support that the superiority and effectiveness of our method on AMOSR under different SNRs of a high openness level.

2) Classification Performance of Different Modulation Types: We provide some confusion matrices of different modulation types achieved by our method on RML.2016.10a dataset in Fig. 7. When SNR = −2dB, Among the known modulation types, there is a confusion between 8PSK and QPSK classification, while the other seven modulation types are classified with good effectiveness. Additionally, our model demonstrates robust discrimination capabilities between known and unknown classes, achieving a recognition accuracy of 94.75% for unknown modulation types. When SNR is at 2dB, our method not only maintains a high accuracy of identifying known modulation types, exceeding 95.00%, but also effectively distinguishes unknown modulation types, achieving a rejection accuracy of 96.00% for them. Similar performances can be observed in the confusion matrix of Fig. 7 (c). These results confirm that PNMP and multi-level feature constraint learning can construct a well-separated feature space for known modulation types while preserving a suitable feature space for unknown modulation types. In Fig. 9, we employ the T-SNE visualization for the signal features. It can be found that our method produces well-separated clusters for known modulation types while reserving sufficient feature space for unknown modulation types. The clusters of known modulation types and those of unknown modulation types are well separable. These findings further verify the effectiveness of the proposed MLFDL under different SNR levels.

In addition, we also give the some confusion matrices achieved by our method on RML.2016.10b dataset in Fig. 8 under the condition of high openness. In Fig. 8 (a), some known modulation signals are misclassified as unknown, among which 8PSK is more misjudged as unknown class with a probability of 79.17%, while the other four known modulation types maintain good classification performance, and the recognition accuracy of unknown category is 73.30%. When SNR = 6dB, the recognition accuracy of 8PSK modulation type signals has been improved from 20.83% to 68.83%, and the recognition accuracy of unknown signals has also been improved from 73.30% to 78.23%. When SNR = 10dB, 8PSK signals and unknown type signals can be distinguished more accurately, with recognition accuracies of 98.50% and 91.22% respectively. The above results support that in the case of high openness, due to the subtle differences in the characteristics between some known modulation types and unknown modulation types, it is challenging to realize the recognition of known modulation classes and the discrimination of unknown modulation classes. Our method can still contribute to enhancing the distinguishability between known and unknown modulation types while maintaining the distinction performance of known modulation classes. In Fig. 10, we provide the visualization results for both known modulation types and unknown modulation types on RML2016.10b dataset. It can be observed that, although under conditions of a large openness level, the feature space occupied by unknown modulation types is larger, the feature space generated based on our method still maintains a relatively sufficient margin from the feature space of known modulation types, enabling the model to effectively distinguish between the known ones and unknown ones.

3) Ablation Study of the Key Design in MLFDL: We conduct ablation study on the key design of the proposed MLFDL.

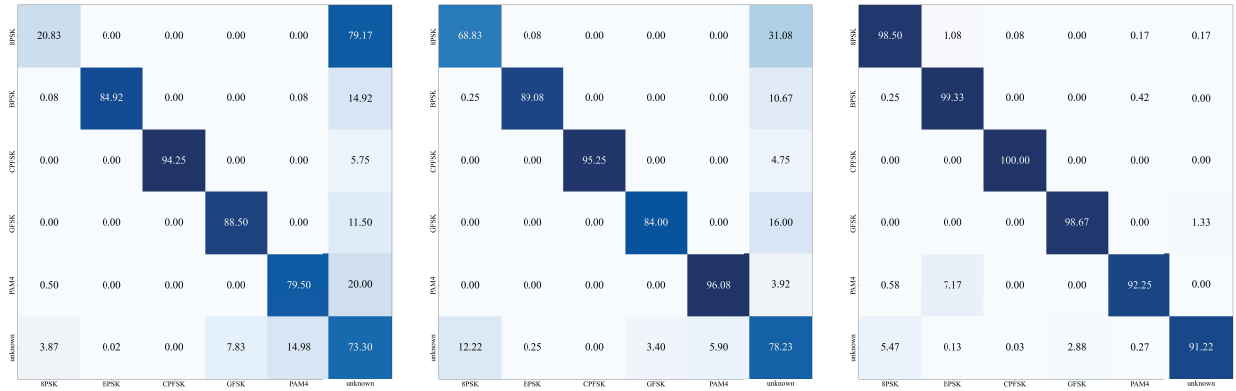

(a) (b) (c)

Fig. 8. Confusion matrices on RML2016.10b for different SNR levels. (a) SNR = 2dB. (b) SNR = 6dB. (c) SNR = 10dB. The vertical axis represents the true label, and the horizontal axis represents the predicted label.

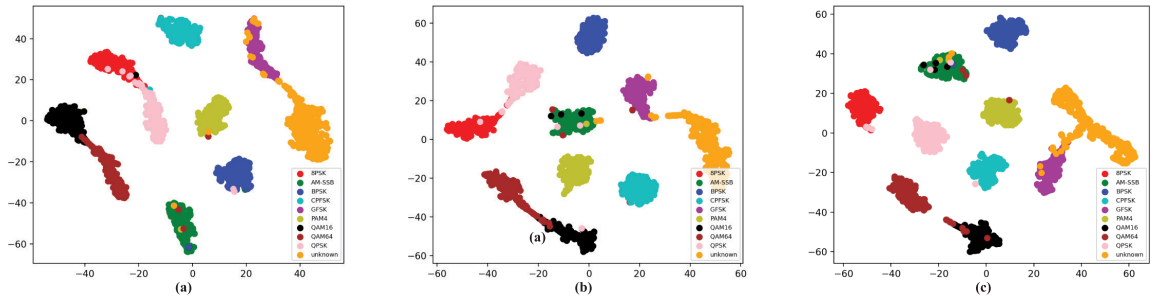

Fig. 9. T-SNE visualization of signal feature embeddings on RML2016.10a under different SNR. (a) SNR = 2dB. (b) SNR = 4dB. (c) SNR = 6dB.

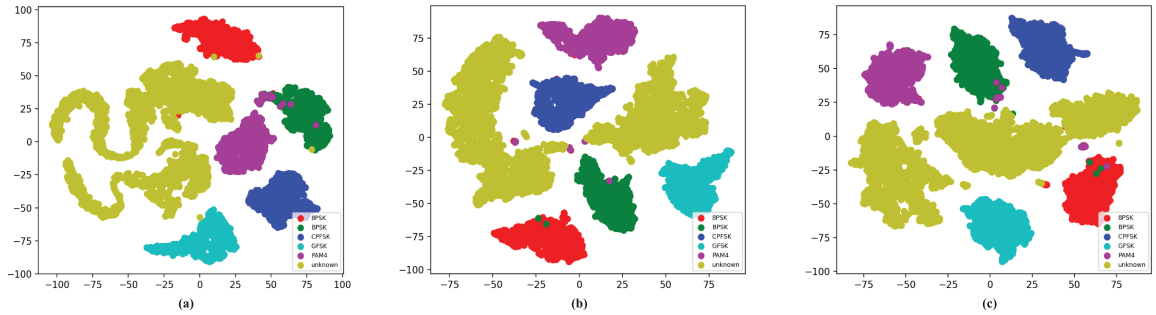

Fig. 10. T-SNE visualization of signal feature embeddings on RML2016.10b under different SNR. (a) SNR = 2dB. (b) SNR = 6dB. (c) SNR = 10dB.

TABLE VIII

THE ABLATION STUDY OF DIFFERENT LOSS COMPONENT WHEN SNR IS 14DB AND OPENNESS IS 18.35% ON RML2016.10B DATASET (%)

$\mathcal{L}_{KMC}$	$\mathcal{L}_{PNMP}$	$\mathcal{L}_{CL}$	$\mathcal{L}_{MMFC}$	AUROC	OSCR	AKS	AUS	NA
✓	×	×	×	79.21	79.02	99.71	73.25	86.48
✓	✓	×	×	83.42	83.25	98.98	81.65	90.31
✓	✓	✓	×	88.82	87.21	98.12	85.54	91.83
✓	✓	×	✓	90.64	90.37	99.55	84.58	92.06
✓	✓	✓	✓	**96.83**	**95.74**	**99.66**	**86.88**	**93.27**

To investigate the contribution of each key component in MLFDL, the loss of each component is gradually added based on the previous group in Table VIII. Specifically, the first group is only optimized by $\mathcal{L}_{KMC}$. The second group is optimized by $\mathcal{L}_{KMC} + \mathcal{L}_{PNMP}$. It can be observed that the introduction of PNMP brings 4.21%, 4.23%, and 3.83% improvements on AUROC, OSCR, and NA, respectively, demonstrating that PNMP effectively expand the feature space for unknown modulation types. The third group is optimized with $\mathcal{L}_{KMC} + \mathcal{L}_{PNMP} + \mathcal{L}_{CL}$, which results in a 5.40% AUROC

TABLE IX
RANDOMLY DIFFERENT UNKNOWN CLASS SETTING

Setting	Known modulation types	Unknown modulation types
1	QPSK, WBFM, CPFSK, GFSK, PAM4, QAM16, QAM64	8PSK, BPSK, AM-DSB
2	8PSK, BPSK, AM-DSB, GFSK, PAM4, QAM16, QAM64	QPSK, WBFM, CPFSK

TABLE X
THE AMOSR PERFORMANCE UNDER DIFFERENT UNKNOWN CLASS CONFIGURATION (%)

Setting	AUROC	OSCR	AKS	AUS	NA
1	94.86	83.46	95.42	94.89	94.80
2	92.32	85.39	95.06	92.45	94.73

improvement and a 3.60% increase in OSCR, verifying that the proposed sample-centroid contrastive learning is conducive to forming a feature space with compact intra-class tightness and strong inter-class separability for known modulated signals and unknown ones. The fourth group is optimized with $\mathcal{L}_{KMC} + \mathcal{L}_{PNMP} + \mathcal{L}_{MMFC}$. Compared to the second group, the introduction of $\mathcal{L}_{MMFC}$ improves AUROC and OSCR by 7.22% and 7.12%, respectively. In the fifth group, we integrate all proposed modules and gain the best performance on all metrics, indicating the proposed PNMP and MFDC can mutually support each other in terms of expanding from unknown spaces and constraining intra-class and inter-class feature distributions, effectively enhancing the performance of AMOSR.

4) Ablation Study of Unknown Diversity: To further verify the effectiveness of MLDFL facing diverse unknown class configuration, we add two ablation experiments to demonstrate the effectiveness of our method confronted with randomly selected unknown modulation types.

As shown in Tables IX and X, our method demonstrates strong performance under different unknown class configurations, maintaining high open-set recognition accuracy. Specifically, the AUROC reaches 94.86% and 92.32%, AKS achieves 95.42% and 95.06%, and AUS attains 94.89% and 92.45% in the two settings, respectively. These results indicate that by integrating PNMP and the multi-level feature constraint, our method effectively distinguishes between known and unknown modulation types. Furthermore, the OSCR achieves 83.46% and 85.39%, NA reaches 94.80% and 94.73%, in the two settings, respectively. These results confirm that our method not only rejects unknown signals effectively but also preserves high modulation recognition accuracy for known signals. Overall, these results validate the robustness and stability of our method in handling the diversity of unknown classes in AMOSR task.

5) AMOSR Performance Under Different Training Stage: To demonstrate the convergence of model performance, under the conditions of RML.2016.10b and SNR = 14dB, we present the AUROC and OSCR results after training for 10, 20, 30, 40, and 50 epochs, respectively, in Fig. 11. It can be observed that as the training progresses, our method consistently improves on both metrics. While accurately rejecting

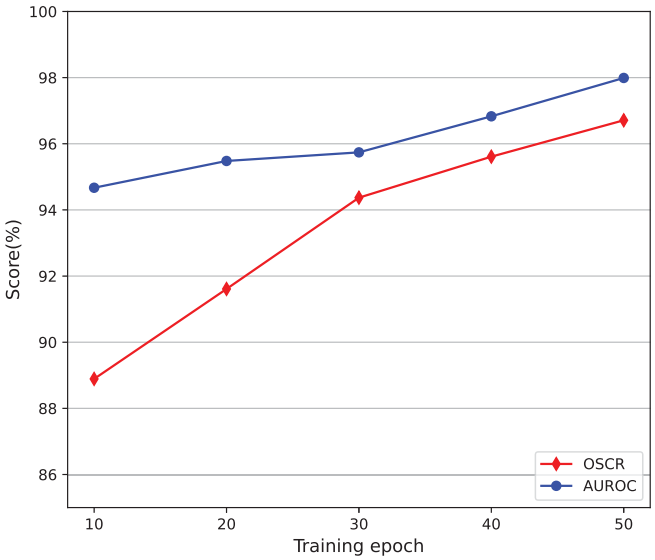

Fig. 11. The AUROC and OSCR performance under different training stage.

TABLE XI
ABLATION STUDY OF λ FOR MANIFOLD MIXUP (%)

Range	AUROC	OSCR	AKS	AUS	NA
$[0, 1)$	95.12	91.03	98.21	85.01	91.61
$[0.25, 1)$	95.48	92.33	98.35	85.12	91.73
$[0.5, 1)$	95.65	91.21	98.28	85.07	91.67
$[0.75, 1)$	96.30	94.90	99.12	86.31	92.71
$[0.98, 1)$	**96.83**	**95.74**	**99.66**	**86.88**	**93.27**

unknown modulation types, it effectively ensures the accuracy of known modulation types. Moreover, the convergence speed is fast; after the training 20 epochs, the AUROC reaches 95.48%, and the OSCR reaches 91.41% After 50 epochs, the AUROC reaches 97.99%, and the OSCR reaches 96.71%. These findings demonstrate that our method achieves effective discrimination between known and unknown modulation types with a fast convergence speed.

6) Sensitivity Analysis of λ in Manifold Mixup: We employ the manifold mixup as Eq. 3 to generate the virtual unknown modulation features using two 1D signals with different modulation types. The range of can determine the similarity between the distribution of the generated pseudo-modulated unknown signals and the distribution of the original unknown modulation types. To this end, we conduct five sets of ablation experiments to analyze the impact of on open-set recognition performance, including $[0, 1)$,$[0.25, 1)$,$[0.5, 1)$,$[0.75, 1)$,and $[0.98, 1)$. As shown in Table XI, adopting mixup with different λ value intervals effectively maintains stable AMOSR performance, achieving

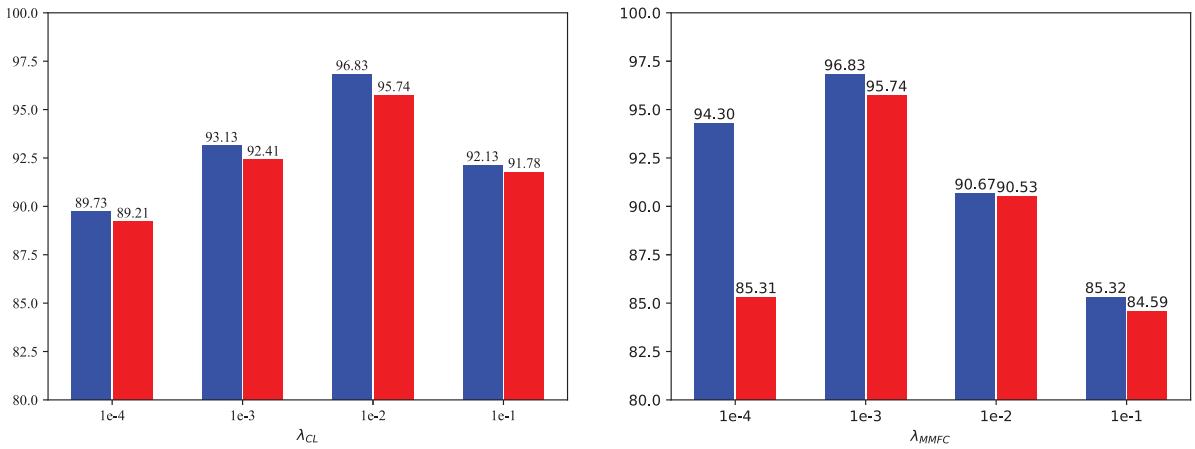

Fig. 12. The ablative results for the loss contribution parameter, subplot (a) for λ_{CL} and subplot (b) for λ_{MMFC}. Blue represents the performance of AUROC, and red represents the performance of OSCR.

an AUROC above 95% and an OSCCR above 91%, which demonstrates the robustness and generalizability of the proposed method across varying mixup augmentation settings. when sampling λ within the range of $[0.98, 1)$, the proposed method achieves optimal performance. This demonstrates that setting to a larger value can generate pseudo-samples that closely resemble the original modulated signals, enhancing the model ability to distinguish unknown modulation features, particularly those that are difficult to differentiate from known modulation signal, resulting in the best AUROC of 96.83% and the highest OSCR of 95.74% among all ablation groups.

7) Ablation Study on the Contribution of the Feature Constraint Loss: To verify the appropriate intensity of feature constraint in the overall loss of Eq. 12, we conduct an ablation study of λ_{CL} and λ_{MMFC} in Eq. 12. Under the condition of SNR = 14dB on RML2016.10b dataset.

First, we conduct ablation experiments on the contribution coefficient of the contrastive loss by setting different λ_{CL} and a fixed λ_{MMFC} of 0.001. The experimental results are presented the second part of Fig. 12. It can be observed that when λ_{CL} is set to 0.1, the AUROC performance and OSCR performance reach their peaks for 96.83% and 95.74, respectively, in the left bar graph of Fig. 12.

Second, we perform AMOSR experiments using the control variable method, with various settings for λ_{MMFC} and a fixed λ_{CL} of 0.1. The ablative results are provided in the right bar graph of Fig. 12. To better balance the magnitude of λ_{MMFC} and prevent it from excessively influencing the classification loss and contrastive learning loss, the proposed method achieves the highest AUROC of 96.83% and OSCR of 95.74% when λ_{MMFC} is set to 0.001. If the magnitude of MMFC is too large, it will have a negative impact on the performance of AUROC and OSCR.

V. Conclusion

In conclusion, we present a novel MLFDL method for AMOSR. The proposed MLFDL method advances open-set modulation recognition through the synergistic integration of the pseudo-modulation placeholder method and multi-level feature distribution constraints. By employing manifold mixup to simulate unknown signal characteristics, coupled with sample-centroid contrastive learning and max-min feature constraints, our approach simultaneously achieves critical objectives: effective modeling of potential unknown modulations, preservation of discriminative feature space organization, and maintenance of optimal intra-class compactness and inter-class separation. Extensive experimental validation demonstrates MLFDL superior performance, with statistically significant improvements in both AUROC and OSCR metrics, underscoring its enhanced generalization capacity and operational robustness in practical open-set scenarios characterized by dynamic signal environments.

One future direction is to develop methods capable of estimating the number of distinct modulation types within the detected unknown categories. Such a capability would enable more comprehensive analysis of emerging signals and provide deeper insight into the communication landscape. In addition, designing incremental modulation recognition methods under low-labeling condition is also crucial for practical scenarios.

References

[1] S. Peng, S. Sun, and Y.-D. Yao, "A survey of modulation classification using deep learning: Signal representation and data preprocessing," *IEEE Trans. Neural Netw. Learn. Syst.*, vol. 33, no. 12, pp. 7020–7038, Dec. 2022.

[2] S. Huang et al., "Automatic modulation classification using gated recurrent residual network," *IEEE Internet Things J.*, vol. 7, no. 8, pp. 7795–7807, Aug. 2020.

[3] P. Oza and V. M. Patel, "C2AE: Class conditioned auto-encoder for open-set recognition," in *Proc. IEEE/CVF Conf. Comput. Vis. Pattern Recognit. (CVPR)*, Jun. 2019, pp. 2307–2316.

[4] Y. Wang, M. Liu, J. Yang, and G. Gui, "Data-driven deep learning for automatic modulation recognition in cognitive radios," *IEEE Trans. Veh. Technol.*, vol. 68, no. 4, pp. 4074–4077, Apr. 2019.

[5] S. Rajendran, W. Meert, D. Giustiniano, V. Lenders, and S. Pollin, "Deep learning models for wireless signal classification with distributed low-cost spectrum sensors," *IEEE Trans. Cognit. Commun. Netw.*, vol. 4, no. 3, pp. 433–445, Sep. 2018.

[6] J. Cai, F. Gan, X. Cao, and W. Liu, "Signal modulation classification based on the transformer network," *IEEE Trans. Cognit. Commun. Netw.*, vol. 8, no. 3, pp. 1348–1357, Sep. 2022.

[7] Y. Li, X. Shi, H. Tan, Z. Zhang, X. Yang, and F. Zhou, "Multi-representation domain attentive contrastive learning based unsupervised automatic modulation recognition," *Nature Commun.*, vol. 16, no. 1, p. 5951, Jul. 2025.

[8] Z. Zhang et al., "A time–frequency-aware hierarchical feature optimization method for SAR jamming recognition," *IEEE Trans. Aerosp. Electron. Syst.*, vol. 61, no. 4, pp. 10619–10635, Aug. 2025.
[9] M. Zhang, P. Tang, G. Wei, X. Ni, G. Ding, and H. Wang, "Open set domain adaptation for automatic modulation classification in dynamic communication environments," *IEEE Trans. Cognit. Commun. Netw.*, vol. 10, no. 3, pp. 852–865, Jun. 2024.
[10] Y. Chen, X. Xu, and X. Qin, "An open-set modulation recognition scheme with deep representation learning," *IEEE Commun. Lett.*, vol. 27, no. 3, pp. 851–855, Mar. 2023.
[11] X. Zhang, T. Li, P. Gong, R. Liu, X. Zha, and W. Tang, "Open set recognition of communication signal modulation based on deep learning," *IEEE Commun. Lett.*, vol. 26, no. 7, pp. 1588–1592, Jul. 2022.
[12] A. Bendale and T. E. Boult, "Towards open set deep networks," in *Proc. IEEE Conf. Comput. Vis. Pattern Recognit. (CVPR)*, Jun. 2016, pp. 1563–1572.
[13] C. F. G. D. Santos and J. P. Papa, "Avoiding overfitting: A survey on regularization methods for convolutional neural networks," *ACM Comput. Surveys*, vol. 54, no. 10s, pp. 1–25, Jan. 2022.
[14] S. Kong and D. Ramanan, "OpenGAN: Open-set recognition via open data generation," in *Proc. IEEE/CVF Int. Conf. Comput. Vis. (ICCV)*, Oct. 2021, pp. 813–822.
[15] K. Katsumata, D. M. Vo, and H. Nakayama, "OSSGAN: Open-set semi-supervised image generation," in *Proc. IEEE/CVF Conf. Comput. Vis. Pattern Recognit. (CVPR)*, Jun. 2022, pp. 11175–11183.
[16] D.-W. Zhou, F. Wang, H.-J. Ye, L. Ma, S. Pu, and D. Zhan, "Forward compatible few-shot class-incremental learning," in *Proc. IEEE/CVF Conf. Comput. Vis. Pattern Recognit.*, Jun. 2022, pp. 9036–9046.
[17] V. Verma et al., "Manifold mixup: Better representations by interpolating hidden states," in *Proc. Int. Conf. Mach. Learn.*, 2019, pp. 6438–6447.
[18] S. Vaze, K. Han, A. Vedaldi, and A. Zisserman, "Open-set recognition: A good closed-set classifier is all you need?" in *Proc. Int. Conf. Learn. Represent.*, 2021, pp. 1–26.
[19] D. Zhang, Y. Lu, Y. Li, W. Ding, B. Zhang, and J. Xiao, "Frequency learning attention networks based on deep learning for automatic modulation classification in wireless communication," *Pattern Recognit.*, vol. 137, May 2023, Art. no. 109345.
[20] J. Zheng and Y. Lv, "Likelihood-based automatic modulation classification in OFDM with index modulation," *IEEE Trans. Veh. Technol.*, vol. 67, no. 9, pp. 8192–8204, Sep. 2018.
[21] B. Dulek, "Online hybrid likelihood based modulation classification using multiple sensors," *IEEE Trans. Wireless Commun.*, vol. 16, no. 8, pp. 4984–5000, Aug. 2017.
[22] E. E. Azzouz and A. K. Nandi, "Procedure for automatic recognition of analogue and digital modulations," *IEE Proc.-Commun.*, vol. 143, no. 5, pp. 259–266, 1996.
[23] L. Han, F. Gao, Z. Li, and O. A. Dobre, "Low complexity automatic modulation classification based on order-statistics," *IEEE Trans. Wireless Commun.*, vol. 16, no. 1, pp. 400–411, Jan. 2017.
[24] B. Ramkumar, "Automatic modulation classification for cognitive radios using cyclic feature detection," *IEEE Circuits Syst. Mag.*, vol. 9, no. 2, pp. 27–45, 2nd Quart., 2009.
[25] C.-S. Park, J. Choi, S. Nah, W. Jang, and D. Y. Kim, "Automatic modulation recognition of digital signals using wavelet features and SVM," in *Proc. Int. Conf. Adv. Commun. Technol.*, 2008, pp. 387–390.
[26] K. Hassan, I. Dayoub, W. Hamouda, and M. Berbineau, "Automatic modulation recognition using wavelet transform and neural networks in wireless systems," *EURASIP J. Adv. Signal Process.*, vol. 2010, no. 1, pp. 1–13, Dec. 2010.
[27] C. Dubuc, D. Boudreau, F. Patenaude, and R. Inkol, "An automatic modulation recognition algorithm for spectrum monitoring applications," in *Proc. IEEE Int. Conf. Commun.*, Jun. 1999, pp. 570–574.
[28] T. J. O'Shea, J. Corgan, and T. C. Clancy, "Convolutional radio modulation recognition networks," in *Proc. 17th Int. Conf. Eng. Appl. Neural Netw.*, 2016, pp. 213–226.
[29] H. Tan, Z. Zhang, Y. Li, X. Shi, and F. Zhou, "Multi-scale feature fusion and distribution similarity network for few-shot automatic modulation classification," *IEEE Signal Process. Lett.*, vol. 31, pp. 2890–2894, 2024.
[30] Z. Liu et al., "Swin transformer: Hierarchical vision transformer using shifted windows," in *Proc. IEEE/CVF Int. Conf. Comput. Vis. (ICCV)*, Oct. 2021, pp. 10012–10022.
[31] Y. Wang, H. Yao, and S. Zhao, "Auto-encoder based dimensionality reduction," *Neurocomputing*, vol. 184, pp. 232–242, Apr. 2016.
[32] Z. Ke and H. Vikalo, "Real-time radio technology and modulation classification via an LSTM auto-encoder," *IEEE Trans. Wireless Commun.*, vol. 21, no. 1, pp. 370–382, Jan. 2022.
[33] A. Ali, F. Yangyu, and S. Liu, "Automatic modulation classification of digital modulation signals with stacked autoencoders," *Digit. Signal Process.*, vol. 71, pp. 108–116, Dec. 2017.
[34] X. Geng, G. Dong, Z. Xia, and H. Liu, "SAR target recognition via random sampling combination in open-world environments," *IEEE J. Sel. Topics Appl. Earth Observ. Remote Sens.*, vol. 16, pp. 331–343, 2023.
[35] C. Wang et al., "An entropy-awareness meta-learning method for SAR open-set ATR," *IEEE Geosci. Remote Sens. Lett.*, vol. 20, pp. 1–5, 2023.
[36] G. Chen, P. Peng, X. Wang, and Y. Tian, "Adversarial reciprocal points learning for open set recognition," *IEEE Trans. Pattern Anal. Mach. Intell.*, vol. 44, no. 11, pp. 8065–8081, Nov. 2022.
[37] B. Xu, F. Shen, and J. Zhao, "Contrastive open set recognition," in *Proc. AAAI Conf. Artif. Intell.*, Jun. 2023, pp. 10546–10556.
[38] Z.-G. Liu, Y.-M. Fu, Q. Pan, and Z.-W. Zhang, "Orientational distribution learning with hierarchical spatial attention for open set recognition," *IEEE Trans. Pattern Anal. Mach. Intell.*, vol. 45, no. 7, pp. 8757–8772, Jul. 2023.
[39] Y. Kong, S. Xia, L. Dong, X. Yu, and G. Cui, "Compound jamming recognition via contrastive learning for distributed MIMO radars," *IEEE Trans. Veh. Technol.*, vol. 73, no. 6, pp. 7892–7907, Jun. 2024.
[40] P. Khosla et al., "Supervised contrastive learning," in *Proc. Adv. Neural Inf. Process. Syst.*, vol. 33, 2020, pp. 18661–18673.
[41] D.-W. Zhou, H.-J. Ye, and D. Zhan, "Learning placeholders for open-set recognition," in *Proc. IEEE/CVF Conf. Comput. Vis. Pattern Recognit.*, Jun. 2021, pp. 4399–4408.
[42] H. Huang, Y. Wang, Q. Hu, and M.-M. Cheng, "Class-specific semantic reconstruction for open set recognition," *IEEE Trans. Pattern Anal. Mach. Intell.*, vol. 45, no. 4, pp. 4214–4228, Apr. 2023.
[43] O. A. Dobre, A. Abdi, Y. Bar-Ness, and W. Su, "Survey of automatic modulation classification techniques: Classical approaches and new trends," *IET Commun.*, vol. 1, no. 2, pp. 137–156, Apr. 2007.
[44] J. Xu, C. Luo, G. Parr, and Y. Luo, "A spatiotemporal multi-channel learning framework for automatic modulation recognition," *IEEE Wireless Commun. Lett.*, vol. 9, no. 10, pp. 1629–1632, Oct. 2020.
[45] G. Chen et al., "Learning open set network with discriminative reciprocal points," in *Proc. Eur. Conf. Comput. Vis.*, 2020, pp. 507–522.
[46] T. J. O'Shea, T. Roy, and T. C. Clancy, "Over-the-air deep learning based radio signal classification," *IEEE J. Sel. Topics Signal Process.*, vol. 12, no. 1, pp. 168–179, Feb. 2018.
[47] H.-M. Yang, X.-Y. Zhang, F. Yin, Q. Yang, and C.-L. Liu, "Convolutional prototype network for open set recognition," *IEEE Trans. Pattern Anal. Mach. Intell.*, vol. 44, no. 5, pp. 2358–2370, May 2022.

Zhenxi Zhang (Member, IEEE) was born in Shandong, China, in 1995. He received the B.Sc. degree in electronic information engineering from Guangxi University, Nanning, China, in 2017, and the Ph.D. degree from the School of Electronic Engineering, Xidian University, in 2022.

He is currently an Associate Professor with the School of Electronic Engineering, Xidian University. His current research interests include electronic reconnaissance, pattern recognition, and computer vision.

Haoyue Tan (Student Member, IEEE) was born in Hebei, China, in 1999. She received the B.Eng. degree in communication engineering from Harbin Engineering University, Harbin, China, in 2021. She is currently pursuing the master's degree in electronic science and technology with the Key Laboratory of Electronic Information Countermeasure and Simulation of the Education Ministry of China, Xidian University.

Her current research interests include automatic modulation classification and deep learning.

Xiaoran Shi (Member, IEEE) was born in Hebei, China, in 1987. She received the Ph.D. degree in signal processing from the National Laboratory of Radar Signal Processing, Xidian University, Xi'an, China, in 2016.

She is currently a Distinguished Professor of electronic science and technology with Xidian University. Her current research interests include deep learning, target recognition, and emitter recognition.

Heng Zhou (Member, IEEE) received the B.Sc. degree in communication engineering from Xi'an University of Posts and Telecommunications, Xi'an, China, in 2018, and the Ph.D. degree in electronics science and technology from Xidian University, Xi'an, China, in 2024.

From 2021 to 2024, he was a joint Ph.D. Student with the Academy of Military Science, Beijing, China. He is currently a Lecturer with the School of Artificial Intelligence and Computer Science, Jiangnan University, Wuxi, China. His current research interests include multi-modal image processing, pattern recognition, and their applications in smart cities and autonomous driving.

Yun Lin (Senior Member, IEEE) received the B.S. degree from Dalian Maritime University, Dalian, China, in 2003, the M.S. degree from Harbin Institute of Technology, Harbin, China, in 2005, and the Ph.D. degree from Harbin Engineering University, Harbin, in 2010. He was a Research Scholar with Wright State University, USA, from 2014 to 2015. He is currently a Full Professor with the College of Information and Communication Engineering, Harbin Engineering University, China. His research interests include machine learning and data analytics over wireless networks, signal processing and analysis, cognitive radio, and software-defined radio.

Yu Li (Graduate Student Member, IEEE) was born in Hotan, Xinjiang Uygur Autonomous Region, in 1999. He received the B.Eng. degree in electronic engineering from Xidian University in 2021. He is currently pursuing the Ph.D. degree in Key Laboratory of Electronic Information Countermeasure and Simulation of the Education Ministry of China, Xidian University. His current research interests include deep learning, cognitive radio, and modulation recognition.

Jiankun Ma was born in Anhui, China, in 2001. He received the bachelor's degree in electronic information engineering from Xidian University in 2023. He is currently pursuing the master's degree with the Key Laboratory of Electronic Information Countermeasure and Simulation, Ministry of Education, Xidian University. His current research interests include deep learning and modulation recognition.

Xueru Bai (Senior Member, IEEE) was born in Xi'an, Shaanxi, China, in 1984. She received the B.S. and Ph.D. degrees in signal and information processing from Xidian University, Xi'an, China, in 2006 and 2011, respectively.

She is currently a Professor with the National Laboratory of Radar Signal Processing, Xidian University. Her research interests include high-resolution radar imaging and radar automatic target recognition. She was a recipient of the National Excellent Doctoral Dissertation Award granted by the Ministry of Education of China and the Program for Excellent Young Scientist selected by the National Natural Science Foundation of China.

Feng Zhou (Member, IEEE) was born in Henan, China, in 1980. He received the M.S. and Ph.D. degrees in signal and information processing from Xidian University, Xi'an, China, in 2004 and 2007, respectively.

He is currently the Dean with the School of Aerospace Space and Technology, Xidian University. His research interests include electronic countermeasures and space electronic information systems. He was granted the Program for New Century Excellent Talents in University in China and he was a recipient of the Young Scientist Award from the XXXI URSI GASS committee.